BIOCHEMISTRY
including biophysical chemistry & molecular biology
Article

*Biochemistry* **2010,** *49,* 6627–6634 6627
DOI: 10.1021/bi100630t

# Iron-Nucleated Folding of a Metalloprotein in High Urea: Resolution of Metal Binding and Protein Folding Events†

Anna Morleo,‡ Francesco Bonomi,‡ Stefania Iametti,‡ Victor W. Huang,§ and Donald M. Kurtz Jr.*,§

‡*DISMA, University of Milan, Via G. Celoria 2, 20133 Milan, Italy, and* §*Department of Chemistry, University of Texas at San Antonio, One UTSA Circle, San Antonio, Texas 78249*

*Received April 26, 2010; Revised Manuscript Received June 22, 2010*

ABSTRACT: Addition of iron salts to chaotrope-denatured aporubredoxin (apoRd) leads to nearly quantitative recovery of its single $Fe(SCys)_4$ site and native protein structure without significant dilution of the chaotrope. This "high-chaotrope" approach was used to examine iron binding and protein folding events using stopped-flow UV−vis absorption and CD spectroscopies. With a 100-fold molar excess of ferrous iron over denatured apoRd maintained in 5 M urea, the folded holo$Fe^{III}$Rd structure was recovered in >90% yield with a $t_{1/2}$ of <10 ms. More modest excesses of iron also gave nearly quantitative holoRd formation in 5 M urea but with chronological resolution of iron binding and protein folding events. The results indicate structural recovery in 5 M urea consists of the minimal sequence: (1) binding of ferrous iron to the unfolded apoRd, (2) rapid formation of a near-native ferrous $Fe(SCys)_4$ site within a protein having no detectable secondary structure, and (3) recovery of the ferrous $Fe(SCys)_4$ site chiral environment nearly concomitantly with (4) recovery of the native protein secondary structure. The rate of step 2 (and, by inference, step 1) was not saturated even at a 100-fold molar excess of iron. Analogous results obtained for Cys → Ser iron ligand variants support formation of an unfolded-$Fe(SCys)_3$ complex between steps 1 and 2, which we propose is the key nucleation event that pulls together distal regions of the protein chain. These results show that folding of chaotrope-denatured apoRd is iron-nucleated and driven by extraordinarily rapid formation of the $Fe(SCys)_4$ site from an essentially random coil apoprotein. This high-chaotrope, multispectroscopy approach could clarify folding pathways of other $[M(SCys)_3]$- or $[M(SCys)_4]$-containing proteins.

Rubredoxins (Rds)[1] constitute a group of small (typically ∼54-residue) bacterial and archaeal non-heme iron electron transfer proteins. Since their discovery in 1965 (*1*), Rds have been among the most thoroughly studied non-heme metalloproteins. More than 50 NMR solution and X-ray crystal structures of Rds have been deposited in the Protein Data Bank. Relevant structural characteristics are shown in Figure 1 for the prototypical Rd from *Clostridium pastuerianum*. These characteristics include an approximately tetrahedral $Fe(SCys)_4$ site surrounded by a pair of iron-ligating CXXC loops sequentially separated from each other by 29 residues, and a $\beta$-sheet containing the N- and C-termini (*2*). The iron site cycles between $Fe^{II}$ and $Fe^{III}$ formal oxidation states. Because of their small size, well-characterized structural and spectroscopic properties, and their extraordinary resistance to denaturation and metal release, numerous investigations of thermal and chaotrope-induced unfolding of and metal loss from Rd have been reported (*3*−*11*). Our recent study (*12*), however, was the first to investigate the opposite process, namely, the polypeptide folding pathway of Rds and the influence of metal ion incorporation on this pathway.

Native cofactors can affect folding rates and pathways of apoproteins. A common approach to measurement of protein folding kinetics is to rapidly dilute a chaotrope-denatured protein below the denaturing chaotrope concentration and monitor buildup of spectral signals associated with the native folded structure (*13*). In the case of the small copper-binding protein, azurin, dilution of the chaotrope-denatured apoprotein with $Cu^{2+}$ solutions led to much faster rates of recovery of the spectroscopically native copper site than when adding $Cu^{2+}$ to nondenatured apoprotein (*14*). We encountered a somewhat different metal incorporation−folding scenario for Rd (*12*). Dilution of chaotrope-denatured apoRd with iron-containing buffer resulted in only a minor portion of native, iron-containing Rd, the major portion consisting of a structured apoRd that was unable to incorporate iron. Under these conditions collapse of the denatured apoRd to an "iron-binding incompetent" structure apparently outcompetes iron binding to the denatured apoprotein. On the other hand, pre-addition of ferric or ferrous salts to chaotrope-denatured apoRd followed by dilution of the chaotrope led to high yields of natively structured $Fe(SCys)_4$-containing Rd. More remarkably, iron-induced folding of Cp apoRd in 6 M urea (well above the apo denaturing midpoint) led to the

†This work was supported by the National Institutes of Health (GM040388, D.M.K.), by the University of Milan (PUR 2007, F.B.), and by MIUR (PRIN 2008, S.I.). A.M. is the grateful recipient of a postdoctoral position from the University of Milan.

*To whom correspondence should be addressed. Phone: (210) 458-7060. Fax: (210) 458-7428. E-mail: donald.kurtz@utsa.edu.

[1]Abbreviations: Rd, rubredoxin; apoRd, metal-free Rd; holoRd, iron-containing Rd in its native folded structure; Cp, *Clostridium pasteurianum*; CD, circular dichroism; wt, wild type; Tris-HCl, tris-(hydroxymethyl)aminomethane hydrochloride; CXXC, two cysteine residues (C) separated by two other residues, X, in the Rd amino acid sequence; C6S, C9S, C39S, and C42S, Cys → Ser variant Rds; unfolded-$Fe^{II}(SCys)_4$, species exhibiting near-UV absorption characteristic of the native $Fe^{II}(SCys)_4$ site but no CD signal for protein secondary structure; chiral-$Fe^{II}(SCys)_4$, species exhibiting near-UV absorption and CD signals characteristic of the native $Fe^{II}(SCys)_4$ site; folded-$Fe^{II}(SCys)_4$, species exhibiting absorption and CD signals for the $Fe^{II}(SCys)_4$ site and the protein secondary structure CD signal characteristic of the native holoRd.


Published on Web 07/08/2010

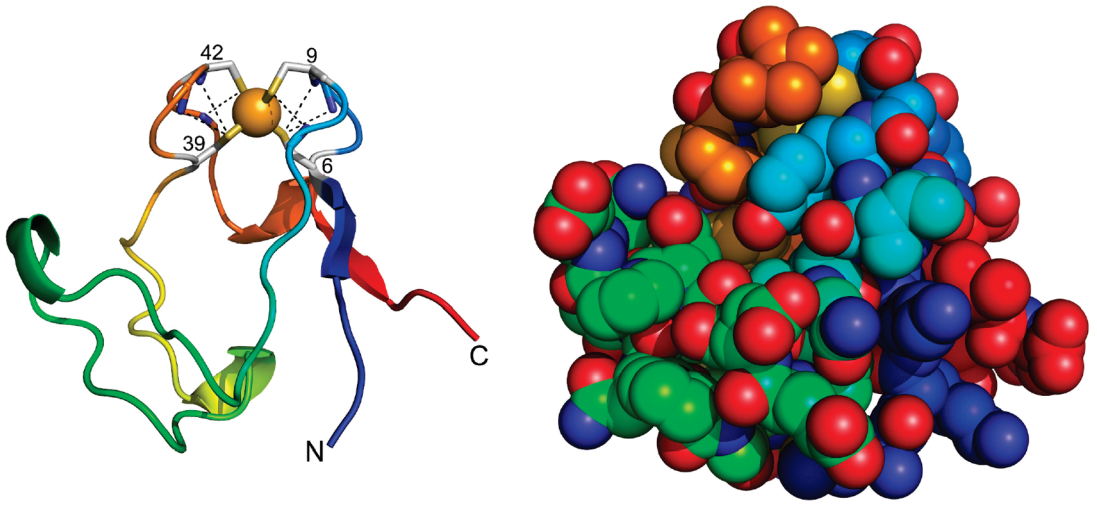


FIGURE 1: Cp holoRd structural representations. The left panels shows the backbone with the iron site shown as a sphere, Cys ligands as sticks with sequence numbers indicated, and backbone N−H···SCys hydrogen bonds as dashed lines. The backbone is color spectrum-traced from blue at the N-terminus to red at the C-terminus. The right panel shows a space-filling view (hydrogen atoms omitted). Drawings were generated using PyMOL (http://www.pymol.org) and coordinates from Protein Data Bank entry 1IRO.

spectroscopically native holoRd structure in nearly quantitative yield without significant dilution of the chaotrope. Analogous results were obtained for the hyperthermostable rubredoxin from *Pyrococcus furious* in 6 M guanidine hydrochloride. We now show that under these seemingly extreme conditions, iron binding and protein folding events can be identified and chronologically distinguished.

## MATERIALS AND METHODS

Chemicals were reagent grade or better. Ultrapure urea was from Sigma Chemical Co. (St. Louis, MO). wt Cp Fe- and apoRds were prepared and quantitated according to published procedures (*6*, *12*, *15*). Plasmids encoding C6S, C9S, C39S, and C42S Rds were prepared by adapting previously described protocols (*6*, *16*). Rds were expressed from plasmid-transformed BL-21(DE3) *Escherichia coli* as described for wt Cp Rd using cell culture temperatures of 37 °C for wt and C9S or 30 °C for C6S, C39S, and C42S following induction of protein expression by isopropyl $\beta$-D-thiogalactoside. The C9S variant was isolated and purified in a manner identical to that described for wt Cp Rd. For the C6S, C39S, and C42S variants, solid urea and 2-mercaptoethanol were added to the soluble portion of the cell lysates under anaerobiosis to final concentrations of 4 M and 10 mM, respectively. These solutions were made 1 mM in ferric ammonium citrate and then slowly diluted anaerobically to 0.4 M urea with 50 mM Tris-HCl (pH 7.4) containing 10 mM 2-mercaptoethanol. The soluble portions were loaded on a DEAE-cellulose column (4 cm × 5 cm) equilibrated with 50 mM Tris-HCl (pH 7.4). Proteins were eluted with the same buffer containing 0.5 M NaCl and further purified by anion-exchange chromatography as previously described for wt Cp Rd (*2*, *17*). Rds in the eluate were detected by dual-wavelength monitoring or, in the case of colorless variants, by sodium dodecyl sulfate−polyacrylamide gel electrophoresis (SDS−PAGE). Using these protocols, the wt and C9S variant Rds were isolated as holo-iron proteins, C42S as partially iron loaded, and C39S and C6S as apoproteins. Metal contents were quantitated by inductively coupled plasma-atomic emission spectrometry at the University of Georgia Chemical Analysis Facility and by mass spectrometry (*12*). ApoRds used for the stopped-flow studies were verified to be metal free by these methods. Anaerobic manipulations were conducted using standard vacuum line techniques with protein and reagent solutions placed in rubber septum-sealed vials and transferred via gastight syringes.

Stopped-flow UV−vis absorption experiments used an SX20 spectrophotometer (Applied Photophysics Ltd.) equipped with a photodiode array detector and a 1 cm optical path length cell. Stopped-flow CD experiments used a Jasco J-810 instrument equipped with a Bio-Logic stopped-flow attachment and a 0.2 cm optical path length cell. Stopped-flow reactions were conducted anaerobically ($N_2$ atmosphere) at room temperature by mixing 10 volumes of apoRd solutions in 50 mM Tris-HCl, 50 mM NaCl (pH 7.4), and 5 M urea with 1 volume of aqueous ferrous ammonium sulfate solutions containing buffer but no urea to give 4.6 M urea after mixing. Iron and protein concentrations are indicated in the figure legends and table footnotes.

## RESULTS

All of the results described here were obtained using recombinant Cp Rd. Urea-denatured apoRd solutions in 50 mM Tris-HCl and 50 mM NaCl (pH 7.4) (hereafter termed buffer) were anaerobically mixed via stopped-flow methods with ferrous ammonium sulfate solutions in buffer without urea. The post-mixing solutions remained at 4.6 M urea, which is more than twice the apo denaturing midpoint of ~2 M urea but well below that required to denature holoRd (see Figures S1 and S2 of the Supporting Information and ref *12*). apoRds used for these experiments were prepared in the presence of 2-mercaptoethanol. However, exogenous thiols were removed prior to the stopped-flow experiments to prevent competition with the apoRd for iron as well as potentially interfering spectral signals from iron−exogenous thiol complexes. The common biological reducing agent, sodium dithionite, was not used because its intense absorbance at 315 nm interfered with the $Fe^{II}(SCys)_4$ site spectral signals, and dithionite was also found to interfere with far-UV CD measurements. Finally, while ferric ammonium citrate can be used quantitatively to recover holoRd from apoRd at high urea concentrations (*12*), the kinetic studies reported here used only ferrous ammonium sulfate to prevent potential complications due to citrate chelate competition, Cys redox, nonspecific binding,

Table 1: Rate Constants $k_{obs}$ ($s^{-1}$) for Spectral Signal Recoveries upon Stopped-Flow Mixing of Denatured wt apoRd with $Fe^{2+}$ in 4.6 M Urea[a]

| Fe/Rd (molar ratio) | $A_{315}$ | $\theta_{315}$ | $\theta_{225}$ | $A_{486}$ | $\theta_{500}$ |
|---|---|---|---|---|---|
| 1.1 | 0.99 (0.01) | 0.14 (0.02) | 0.13 (0.01) | 0.020 (0.001) | 0.0073 (0.0007) |
| 11 | 8.96 (0.17) | 0.79 (0.15) | 0.98 (0.18) | 0.039 (0.001) | 0.012 (0.002) |
| 110 | > 100 | > 100 | > 100 | > 100[b] | 0.107 |

[a]Ten volumes of 55 $\mu$M apoRd in 50 mM Tris-HCl (pH 7.4) and 5 M urea were mixed with 1 volume of 0.6, 6, or 60 mM ferrous ammonium sulfate solutions in the same buffer without urea. Rate constants were determined from fits of first-order exponentials to the spectral signal change vs time data exemplified by those shown in Figure 3. Listed values (standard deviations in parentheses) are averages from three to five repetitions. Absorbance time courses were corrected for those recorded upon anaerobic stopped-flow mixing of the same volume ratios of buffered ferrous ammonium sulfate with buffered 5 M urea solutions in the absence of protein. [b]See Figure S7 of the Supporting Information.

and hydrolytic chemistry of $Fe^{3+}$. Unless otherwise indicated, the results reported here were obtained in 4.6 M urea to compare the behavior of wt Rd with those of variants in which the Cys ligand residues were individually changed to Ser (wt Cp Rd contains no other Cys residues and no Ser residues).

Five independent and characteristic spectral signals were used to monitor recovery of the native wt holoRd structure. These spectral signatures (with abbreviations used in Table 1 listed in parentheses) are (i) absorption maxima at ~315 and 335 nm for the $Fe^{II}(SCys)_4$ site ($A_{315}$) (*15*), (ii) negative ellipticity at 315 nm for the $Fe^{II}(SCys)_4$ site ($\theta_{315}$) (*18*, *19*), (iii) negative ellipticity at 225 nm, indicative of protein secondary structure ($\theta_{225}$) (*12*), (iv) absorption features at ~350, 380, 490, and 570 nm for the $Fe^{III}(SCys)_4$ site ($A_{486}$) (*1*), and (v) negative ellipticity at ~500 nm for the $Fe^{III}(SCys)_4$ site ($\theta_{500}$) (*1*). Appropriately designed synthetic CXXC-containing peptides (12−16 residues) form $Fe(SCys)_4$ complexes displaying near-UV−visible absorption and CD features closely resembling those of holoRd, indicating that these features are characteristic of the electronic structure and local environment of the $Fe(SCys)_4$ site (*19*−*21*). These iron site spectral features are retained for holoRd in 4.6 M urea (see Figure S1 of the Supporting Information). wt apoRd shows no near-UV or visible absorption or CD spectra. It does, however, exhibit a far-UV CD spectrum characterized by negative ellipticity at 225 nm, indicating that the apoprotein retains considerable secondary structure in the absence of the chaotrope (*12*). The apoRd far-UV CD spectrum gradually disappears with increasing urea levels. At 4.6 M urea, the far-UV CD signal of apoRd is completely lost, whereas the corresponding holoRd signal is retained (see Figure S2 of the Supporting Information and ref *12*). The aforementioned spectral signals can, thus, be used to monitor discrete iron incorporation and protein folding events.

UV−vis absorption spectral time courses obtained upon anaerobic stopped-flow mixing of wt apoRd with $Fe^{2+}_{(aq)}$ in apo denaturing urea are shown in Figure 2, and corresponding rate constants are listed in Table 1. The first detected absorption feature is the near-UV double maximum characteristic of the pseudotetrahedral $Fe^{II}(SCys)_4$ site, which then more slowly and cleanly converts to the intense visible absorption features of the corresponding $Fe^{III}(SCys)_4$ site. As one can see in Table 1, the rates of this initial $Fe^{II}(SCys)_4$ site spectral recovery increased at least 10-fold with 11-fold increases in $Fe^{2+}$ concentration and showed no evidence of saturation with a molar excess of iron of up to 110-fold (at which the rates were too fast to measure by stopped-flow methods). Figures 2 and 3 show that the $A_{315}$ intensity reaches a maximum and then decreases as the $Fe^{II}(SCys)_4$ site is converted to the $Fe^{III}(SCys)_4$ site. The $A_{315}$ rate constants listed in Table 1 were determined from the earlier portions of the time courses. We attribute the slower appearance

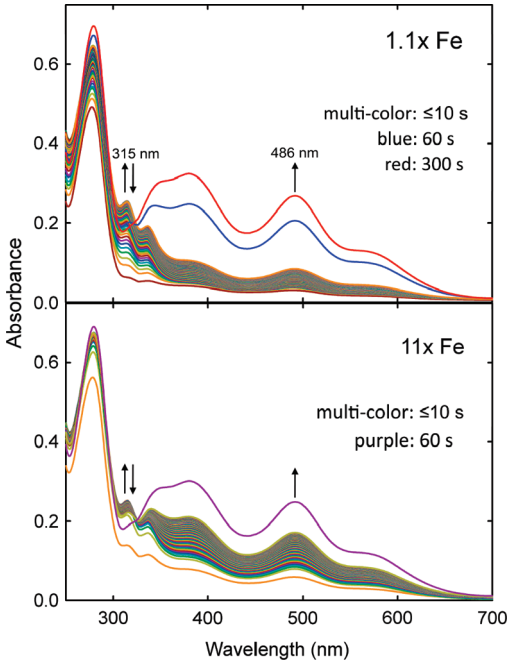


FIGURE 2: UV−vis absorption spectral time courses upon anaerobic stopped-flow mixing of 10 volumes of 55 $\mu$M apoRd in buffer and 5 M urea with 1 volume of either 0.6 (1.1× Fe) or 6 mM (11× Fe) ferrous ammonium sulfate in buffer. For the 10 s time courses, spectra were recorded from 100 ms to 10 s at 100 ms intervals following the mixing dead time (~3 ms). Arrows indicate directions of absorbance changes.

of the native $Fe^{III}(SCys)_4$ site absorption features in Figure 2 ($A_{486}$ in Table 1) to artifactual oxidation by impurities in the concentrated urea solutions, and excess iron may catalyze this oxidation. Figure S3 of the Supporting Information shows that oxidizing impurities in urea also accelerate anaerobic $Fe^{2+}_{(aq)}$ oxidation in the absence of protein.[2] Although the buildup of the $Fe^{III}(SCys)_4$ site absorption could be attributed to the presence of residual dissolved $O_2$, we have repeated these experiments several times (at least five repetitions for the absorbance changes exemplified in Figure 2 over a period of more than one year) with highly reproducible rate constants, including the $Fe^{2+}$ concentration dependence, as well as absorption intensities. Recoveries of the $Fe^{II}(SCys)_4$ site chiral environment ($\theta_{315}$) and protein secondary structure ($\theta_{225}$) clearly lag behind that of the initial $Fe^{II}(SCys)_4$ absorption ($A_{315}$) recovery. The spectra of the $Fe^{III}(SCys)_4$ site ($A_{486}$ and $\theta_{500}$) attributed to artifactual oxidation were the slowest to recover. Representative single-wavelength time courses for all five signal recoveries are

[2]For this reason, urea was omitted from the ferrous ammonium sulfate stock solutions used in the stopped-flow experiments.

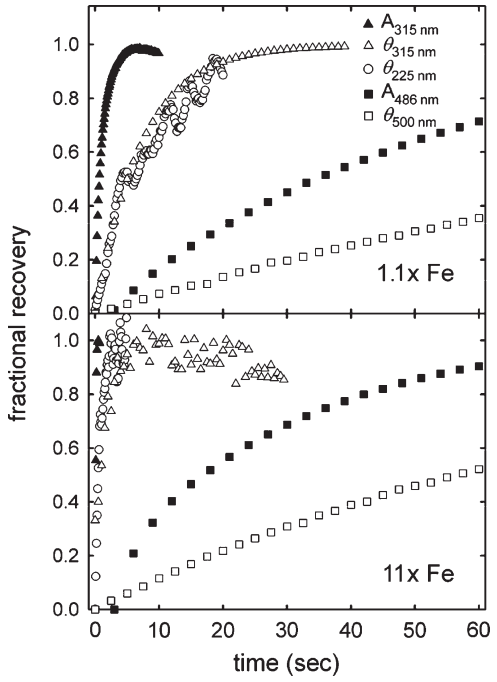


FIGURE 3: Single-wavelength time courses for the spectral signal recoveries upon anaerobic stopped-flow mixing of apoRd in 5 M urea with ferrous ammonium sulfate as described in the legend of Figure 2. Background iron oxidation time courses have been subtracted where appropriate.

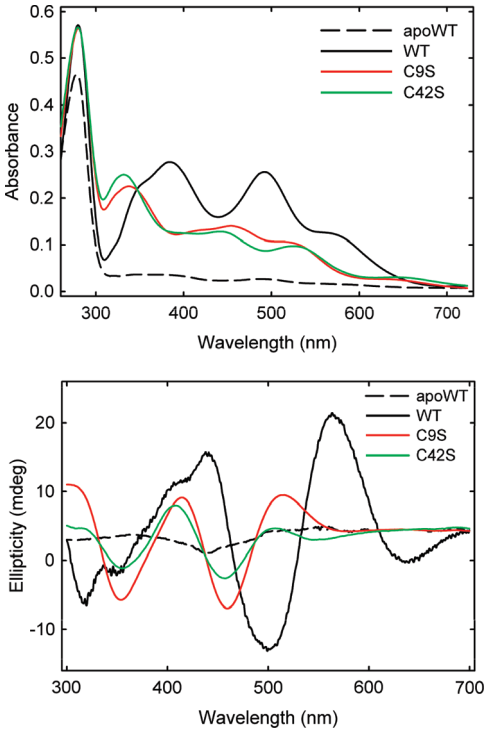


FIGURE 4: Static UV−vis absorption (top) and visible CD (bottom) spectra following anaerobic stopped-flow mixing of 10 volumes of 55 $\mu$M wt, C9S, or C42S apoRd in buffer and 5 M urea with 1 volume of 0.6 mM ferrous ammonium sulfate in buffer (1.1-fold molar excess of iron over protein). wt apoRd spectra without added iron are shown for comparison.

plotted in Figure 3. Semilog plots of the time courses shown in Figure 3 (Figure S4 of the Supporting Information) demonstrate reasonable first-order behavior for all these spectral changes well beyond the half-times. Figure S5 of the Supporting Information shows that the $\theta_{225}$ kinetic trace in Figure 3 (11-fold excess of iron) nearly exactly spans the range of ellipticities between those of static spectra recorded in high urea for unfolded apoRd and folded holoRd at the end of the time course after iron addition. Thus, essentially none of the secondary structure recovery occurred within the stopped-flow mixing dead time, which reinforces the conclusion that this recovery lags behind formation of the $Fe^{II}(SCys)_4$ site.

The four individual Cys → Ser Rd variants, C6S, C9S, C39S, and C42S, have been previously characterized (*22*, *23*). In the absence of the chaotrope, the ferric forms are stable, but the ferrous forms tend to lose iron. As shown in Figure S2 of the Supporting Information, all but the C9S apoRd have lost all detectable secondary structure in 4.6 M urea. The C9S apoRd retains ~30% of its native secondary structure signal at 4.6 M urea for reasons that are not immediately obvious. Figure 4 shows the final static UV−vis absorption and CD spectra obtained following stopped-flow mixing of C9S and C42S apoRds in 4.6 M urea with $Fe^{2+}_{(aq)}$, and Figure 5 shows the corresponding stopped-flow UV−vis absorption time courses. The final spectra are remarkably similar in both shape and intensity to those reported previously for these variants in the absence of chaotrope and have been well established to arise from $Fe^{III}(SCys)_3(OSer)$ sites (*22*). Using the published extinction coefficients, the C9S and C42S holoRd recoveries exceeded 85% in 4.6 M urea. The very earliest portions of the time courses in Figure 5 exhibit weak, relatively narrow absorption features near 320 nm, possibly attributable to $Fe^{II}(SCys)_3$ sites, superimposed on the intense $Fe^{III}(SCys)_3(OSer)$ site absorption. Oxidation to $Fe^{III}(SCys)_3(OSer)$ by urea impurities is apparently extremely rapid following the initial $Fe^{2+}$ binding events. This rapid oxidation is not unexpected (*23*) and is, in fact, an advantage in these experiments because of the aforementioned lability of $Fe^{2+}$ in the Cys → Ser variants. Figure 6 shows single-wavelength absorption and CD spectral time courses for C9S and C42S. The corresponding semilog plots in Figure S6 of the Supporting Information show reasonable first-order behavior, and the rate constants are listed in Table 2. As is the case for the wt protein, $Fe^{III}(SCys)_3(OSer)$ site recovery ("visible absorbance" in Figure 6 and Table 2) is significantly faster than secondary structural recovery ($\theta_{225}$); the $Fe^{III}(SCys)(OSer)$ site chiral environment ("visible CD") is the last to recover but does so only slightly more slowly than secondary structure. The corresponding stopped-flow experiments with the C6S and C39S variants in 4.6 M urea showed the same progression of iron binding and protein folding events on scales similar to those of C9S and C42S but often resulted in relatively lower yields of holoprotein. Kinetic data are, therefore, not reported for C6S and C39S.

## DISCUSSION

All of the rate constants and recovery times reported in this work were obtained in 4.6 M urea; i.e., they are not extrapolated to zero denaturant concentration. With a 110-fold molar excess of $Fe^{2+}$ over apoRd, the spectral signals characteristic of the native folded holo$Fe^{III}$Rd were recovered nearly quantitatively with a $t_{1/2}$ of < 10 ms in 4.6 M urea (see Table 1 and Figure S7 of the Supporting Information). This short time scale includes the apparently artifactual urea-induced oxidation of the ferrous to ferric $Fe(SCys)_4$ site. Such short time scales are unusual if not unique for metal incorporation and protein folding at such high chaotrope concentrations.

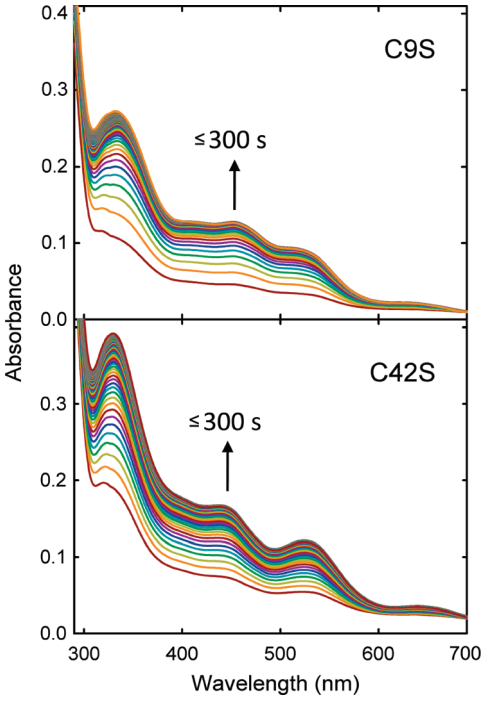


FIGURE 5: UV−vis absorption spectral time courses upon anaerobic stopped-flow mixing of C9S or C42S apoRd in 5 M urea with ferrous ammonium sulfate as described in the legend of Figure 4. Spectra were obtained from 3 to 300 s at 3 s intervals following the mixing dead time (~3 ms). Arrows indicate the direction of absorbance changes.

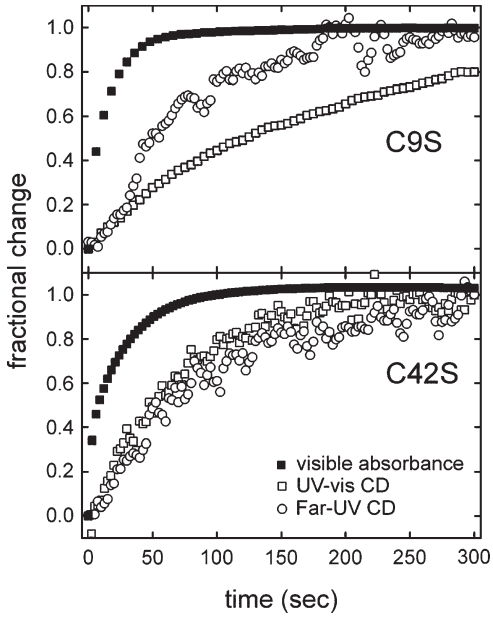


FIGURE 6: Single-wavelength time courses for spectral signal recoveries upon anaerobic stopped-flow mixing of C9S or C42S apoRds in 5 M urea with ferrous ammonium sulfate as described in the legend of Figure 4. Wavelengths used to monitor signal recoveries are listed in the footnote of Table 2. Background iron oxidation time courses have been subtracted where appropriate.

Table 2: Rate Constants $k_{obs}$ ($s^{-1}$) for Spectral Signal Recoveries upon Stopped-Flow Mixing of Denatured C9S and C42S apoRds with $Fe^{2+}_{(aq)}$ in 4.6 M Urea[a]

| Rd variant | Fe/Rd (molar ratio) | visible absorbance | $\theta_{225}$ | visible CD |
|---|---|---|---|---|
| C9S | 1.1 | 0.087 (0.018) | 0.015 (0.002) | 0.006 (0.001) |
| | 11 | 0.91 (0.04) | 0.035 (0.007) | 0.023 (003) |
| C42S | 1.1 | 0.055 (0.002) | 0.013 (0.004) | 0.016 (0.005) |
| | 11 | 0.45 (0.03) | 0.090 (0.011) | 0.041 (0.006) |

[a]Mixing conditions are described in the legend of Figure 4. Rate constants were determined as described in Table 1 from time courses exemplified in Figure 6. Wavelengths used for visible absorbance changes were 433 nm for C9S and 454 nm for C42S. Absorbance time courses were corrected for those recorded upon mixing the same concentrations of ferrous ammonium sulfate and urea in the absence of protein. Wavelengths used for visible range CD time courses were 460 nm for C9S and 458 nm for C42S.

An equally noteworthy outcome is that, at more modest excesses of $Fe^{2+}_{(aq)}$ (1.1 and 11 Fe/Rd molar ratios), iron binding and protein folding events in apo denaturing urea could be chronologically resolved on the stopped-flow time scale. Under these conditions, the first observable spectral signal (double maximum at 315 and 335 nm in Figure 1; $A_{315}$ in Figure 3 and Table 1) is remarkably similar to that of the as-isolated holo-$Fe^{II}$Rd in the absence of chaotrope, despite the lack of any detectable secondary structure. We, therefore, refer to this initially detectable spectral species as unfolded-$Fe^{II}(SCys)_4$. Subsequent recoveries of both the chiral environment around the $Fe^{II}(SCys)_4$ site ($\theta_{315}$) and protein secondary structure ($\theta_{225}$) were significantly slower than formation of unfolded-$Fe^{II}(SCys)_4$. The $Fe^{II}(SCys)_4$ site chiral environment recovery presumably involves local reorganization of the CXXC loops, perhaps including formation or strengthening of the peptide N−H···SCys hydrogen bonds shown in Figure 1.

The rate of unfolded-$Fe^{II}(SCys)_4$ formation ($A_{315}$, $k_{obs}$ in Table 1) showed no evidence of saturation up to a 110-fold molar excess of $Fe^{2+}$. This observation does not support a mechanism involving a rate-determining conformational change of the denatured apoRd. Our results instead support an iron-nucleated folding pathway. The chelate effect of the fluctuating, effectively random coil protein chain would promote rapid formation of unfolded-$Fe^{II}(SCys)_4$ upon $Fe^{2+}$ binding to any one of the four Cys residues. No spectral signals or induction period that can be assigned to a prior unfolded-$Fe^{II}(SCys)_{n<4}$ species were observed, presumably because the initial $Fe^{2+}$ binding event is the slow step in formation of unfolded-$Fe^{II}(SCys)_4$. On the basis of Cys ligand proximity, chemically reasonable committed events leading to the unfolded-$Fe^{II}(SCys)_4$ complex would include formation of a bidendate $Fe^{II}(SCys)_2$ chelate involving either the N- or C-terminal CXXC pair followed by the key nucleation event, namely, binding of a third Cys residue from the other CXXC pair, thereby pulling together the distal portions of the protein chain. A schematic model consistent with the proposed sequential Cys ligation leading to unfolded-$Fe^{II}(SCys)_4$ is shown in Figure 7. At modest excesses of iron, the $k_{obs}$ values for recoveries of chiral-$Fe^{II}(SCys)_4$ ($\theta_{315}$) and folded-$Fe^{II}(SCys)_4$ ($\theta_{225}$) were dependent on the initial $Fe^{2+}_{(aq)}$ concentration, albeit less so than the formation of the initial unfolded-$Fe^{II}(SCys)_4$ (see Table 1). This behavior would be expected under conditions where the $k_{obs}$ for formation of unfolded-$Fe^{II}(SCys)_4$ is within a factor of 10 greater than the inherent first-order rate constants for the subsequent internal folding events.[3]

[3]For at least the ≥11-fold excesses of iron, dissociation of $Fe^{2+}$ from the protein is likely to be slow compared to the forward processes leading to folded-$Fe^{II}(SCys)_4$.

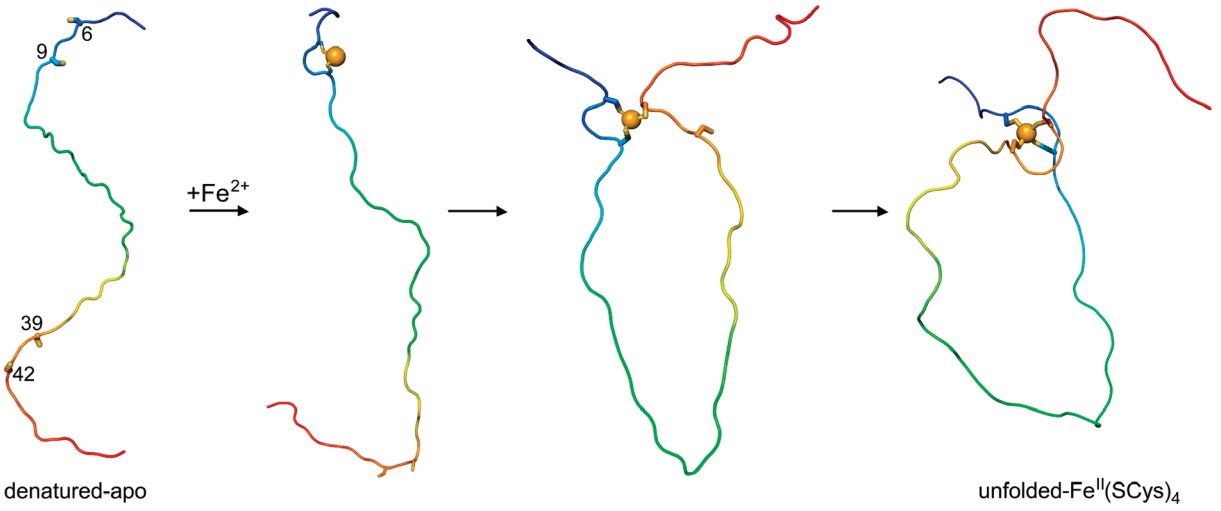


FIGURE 7: Schematic model for the sequential Cys ligation of denatured apoRd leading to unfolded-$Fe^{II}(SCys)_4$ at high urea concentrations. The protein chains are not depicted to uniform scale. Iron is represented as a sphere. The denatured-apo likely consists of an ensemble of fluxional structures. The choice of the Cys6/Cys9 rather than the Cys39/Cys42 residue pair as the initial iron chelate is arbitrary.

An alternative mechanism in which the four Cys residues of the apoRd are preconfigured toward formation of the $Fe(SCys)_4$ site in 4.6 M urea is not supported well by our results. The far-UV CD spectrum of apoRd in 4.6 M urea is consistent with that expected for a random coil (*8*, *19*, *24*) and greatly exceeds the 2 M urea midpoint for loss of detectable secondary structure (see Figure S2 of the Supporting Information) (*12*). Higher urea concentrations do not significantly change the outcome. Iron-initiated folding of wt apoRd in 5.5 M urea is essentially quantitative and occurs with the same progression of spectral signal recoveries and similar time scales as in 4.6 M urea (*12*). It is not clear which intraprotein interactions could stabilize preconfiguration of the four Cys residues in a 54-residue protein having a 29-residue spacing between CXXC pairs while showing no detectable secondary structure and essentially no urea dependence above the denaturation midpoint. Also, we would expect preconfigured apoRd to be retained or its level to be increased upon chaotrope dilution, but as we observed previously (*12*), dilution of chaotrope-denatured apoRd results in a high percentage of iron-uptake incompetent apoprotein.

An iron nucleation pathway for structural recovery of the holoRd is further supported by results of parallel experiments on the C9S and C42S Rds. For these variants, a ferric rather than ferrous unfolded-$Fe(SCys)_3(OSer)$ was the first clearly discernible spectral species. This result is consistent with the much more negative $Fe^{III}/Fe^{II}$ reduction potentials of the Cys → Ser variants (*23*) and with the much higher affinity of the serine side chain for $Fe^{III}$ relative to $Fe^{II}$. Thus, formation of the initial unfolded-$Fe^{III}(SCys)_3(OSer)$ complex is inferred to be equivalent to that of the less iron oxidation prone wt unfolded-$Fe^{II}(SCys)_4$ complex. The rate of formation of the initial unfolded-$Fe^{III}(SCys)_3(OSer)$ increased ~10-fold with a 11-fold increase in $Fe^{2+}$ concentration (Table 2), and formation of this initial complex can be chronologically distinguished from subsequent recoveries of secondary structure and the chiral environment of the $Fe^{III}(SCys)_3(OSer)$ site. These results are consistent with a sequence of rate-determining $Fe^{2+}$ binding to the denatured apo C9S and C42S variants, formation of a transient unfolded-$Fe^{II}(SCys)_3$ complex, and then rapid iron oxidation and Ser ligation, generating the initially observed unfolded-$Fe^{III}(SCys)_3(OSer)$. At the same excesses of iron, formation of the Cys → Ser variant unfolded-$Fe(Cys)_3(OSer)$ is invariably slower than formation of wt unfolded-$Fe^{II}(SCys)_4$ (compare $A_{315}$ $k_{obs}$ in Table 1 vs "visible absorbance" $k_{obs}$ in Table 2). Presuming Ser ligation to $Fe^{2+}$ does not occur, we expect these slower formation rates for one fewer Cys ligand and rate-limiting $Fe^{2+}$ binding leading to unfolded-$Fe^{II}(SCys)_3$. Dissociation of $Fe^{2+}$ from the unfolded-$Fe^{II}(SCys)_3$ C9S, or C42S variants may also kinetically compete with oxidation to the unfolded-$Fe^{III}(SCys)_3(OSer)$ complex, but formation of the spectroscopically native $Fe^{III}(SCys)_3(OSer)$ site is nearly quantitative at the end of the time course. At an Fe/Rd molar ratio of 1.1, the wt unfolded-$Fe^{II}(SCys)_4$ forms at nearly the same rate as does the C92 or C42S unfolded-$Fe^{III}(SCys)_3(OSer)$ at an Fe/Rd molar ratio of 11. At these comparable unfolded-iron complex formation rates, subsequent recovery of secondary structure for the Cys → Ser variants is slower, but within an order of magnitude of that for wt. These comparable time scales indicate that the initially formed $Fe^{III}(SCys)_3(OSer)$ site is somewhat but not dramatically less efficient than the initial $Fe^{II}(SCys)_4$ site at promoting secondary structure recovery. Unlike C42S, C9S apoRd retains ~30% of its chaotrope-free secondary structure in 4.6 M urea. At 8 M urea, C9S apoRd has no detectable secondary structure (see Figure S2 of the Supporting Information) yet still recovers its folded holo$Fe^{III}$Rd structure in >80% yield on a time scale similar to that in 4.6 M urea (F. Bonomi, A. Morleo, S. Iametti, and D. M. Kurtz, Jr., unpublished observations). This folding at extraordinarily high urea levels, together with the detection of unfolded-$Fe^{III}(SCys)_3(OSer)$ and its $Fe^{2+}$ concentration-dependent $k_{obs}$ of formation (Table 2), provides additional support for an iron nucleation over an apo preconfiguration mechanism.

The same sequence of iron binding and folding events was observed for the C6S and C39S variants in 4.6 M urea, but the recovery yields were lower and more variable than for C9S and C42S. The lower yields for C6S and C39S are likely due to the relative instabilities of their $Fe^{II}(SCys)_3$ complexes and the inability of Ser6 and Ser39 to outcompete solvent as the fourth ligand to unfolded-$Fe^{III}(SCys)_3$. The as-isolated C6S variant was previously shown to contain a $Fe^{III}(SCys)_3(OH)$ site, i.e., hydroxo rather than Ser as the fourth ligand at pH 7 in the absence of chaotrope (*23*). Cys6 and Cys39 are relatively buried compared to Cys9 and Cys42 in the native holoRd (see Figure 1) and,

thus, have a greater number of intraprotein contacts. The buried Cys ligands each have two peptide N−H···SCys hydrogen bonds versus only one for the surface Cys ligands (see Figure 1). The burial and iron ligation of Ser6 and Ser39 may, therefore, require a larger number of non-native protein structural accommodations than for the surface-exposed Ser9 and Ser42. These differences could be magnified at high urea concentrations because of weakening of compensating native interactions elsewhere in the protein.

These results suggest that any three of the four Cys residues are sufficient to achieve the initial iron nucleation event, but that a fourth protein side chain ligand at the Cys residue positions is required to achieve the folded native structure in apo denaturing urea. We, thus, propose the minimal metal nucleation−folding sequence for the wt Cp Rd at high urea concentrations: $Fe^{2+}_{(aq)}$ + denatured apo → unfolded-$Fe^{II}(SCys)_3$ → unfolded-$Fe^{II}(SCys)_4$ → chiral-$Fe^{II}(SCys)_4$ → folded-$Fe^{II}(SCys)_4$. In this sequence, the three-Cys ligated species, [unfolded-$Fe^{II}(SCys)_3$], is an unobservable transient intermediate. While secondary structure and $Fe^{II}(SCys)_4$ chiral environment recoveries were monitored independently of each other, they were not chronologically well separated in the wt protein; these two protein structural changes may occur concomitantly. The unfolding curves of the apoRds (Figure S2 of the Supporting Information) do not seem to fit a two-state equilibrium. We do not know whether this behavior is kinetically or thermodynamically controlled. On the other hand, we detected no intermediate secondary structural signals at any point in the iron binding−folding time courses in apo denaturing urea. These results imply that iron nucleates a two-state unfolded- to folded-$Fe(SCys)_4$ conversion. Remarkably, we observe no spectral perturbations for the native wt holoRd even in 8 M urea and so cannot verify a two-state equilibrium unfolding curve for holoRd.

The results provide convincing evidence for iron-nucleated folding of apoRd in apo denaturing chaotrope driven by the extraordinarily rapid formation of the pseudotetrahedral $M(SCys)_4$ site from an essentially random coil apoprotein (*21*). The use of apo denaturing/metal-folded chaotrope levels and spectral signals that independently monitor metal- and protein-centered processes could conceivably be applied to clarify metal-induced folding pathways of other proteins that bind spectroscopically active metal ions, particularly those containing $[M(SCys)_3]$ or $[M(SCys)_4]$ sites (*25*−*27*) or rubredoxin-like $M(SCys)_4$ domains (*28*−*31*), where M is a di- or trivalent metal ion.

The extent to which our results apply to holoRd formation in vivo is uncertain. Iron insertion could be temperature-dependent; the apoRd structure is lost at a much lower temperature than that of holoRd (*24*). Overexpression of Cp Rd in *E. coli* (which contains no native Rd) at 37 °C yields high levels of natively folded iron- or zinc-containing holoRd (*2*, *6*, *32*). $Zn^{2+}$ has an inherently higher affinity than $Fe^{2+}$ for the $M(SCys)_4$ site of Rd (*33*), but Rds isolated directly from parent organisms have never been reported to contain zinc. Intracellular metal ion availability and competing complexation may, therefore, affect the metal content of Rd in the parent organisms. In vivo iron donors to Rd are unknown. In this regard, high yields of holo$Fe^{III}$Rd recovery in apo denaturing urea were unaffected by either exogenous thiols or the use of ferric citrate in place of ferrous salts (*12*). Other intracellular effects, such as macromolecular crowding and altered water structure, could modulate the apoRd iron incorporation and protein folding pathways (*34*−*36*). A possibility suggested by our results is that nucleation of Rd polypeptide folding is initiated prior to dissociation of the apoprotein from the ribosome when any three of the Cys residues become accessible to metal ions (*37*).

## SUPPORTING INFORMATION AVAILABLE

Near-UV CD spectra of apo- and holoRds at high urea concentrations, plots of midpoint urea denaturations of apoRds, spectral time courses of ferrous ammonium sulfate oxidations in 5 M urea, static far-UV CD spectra of apo- and holoRds at high urea concentrations, semilog plots of the time courses in Figures 3 and 6, and stopped-flow absorption spectral time course for apoRd with a 110-fold molar excess of iron in 4.6 M urea. This material is available free of charge via the Internet at http://pubs.acs.org.

## REFERENCES


1. Lovenberg, W., and Sobel, B. E. (1965) Rubredoxin: A new electron transfer protein from *Clostridium pasteurianum*. *Proc. Natl. Acad. Sci. U.S.A. 54*, 193–199.
2. Richie, K. A., Teng, Q., Elkin, C. J., and Kurtz, D. M., Jr. (1996) 2D $^1$H and 3D $^1$H-$^{15}$N NMR of zinc-rubredoxins: Contributions of the $\beta$-sheet to thermostability. *Protein Sci. 5*, 883–894.
3. Cavagnero, S., Zhou, Z. H., Adams, M. W., and Chan, S. I. (1998) Unfolding mechanism of rubredoxin from *Pyrococcus furiosus*. *Biochemistry 37*, 3377–3385.
4. LeMaster, D. M., and Hernandez, G. (2005) Additivity in both thermodynamic stability and thermal transition temperature for rubredoxin chimeras via hybrid native partitioning. *Structure 13*, 1153–1163.
5. Henriques, B. J., Saraiva, L. M., and Gomes, C. M. (2006) Combined spectroscopic and calorimetric characterisation of rubredoxin reversible thermal transition. *J. Biol. Inorg. Chem. 11*, 73–81.
6. Eidsness, M. K., Richie, K. A., Burden, A. E., Kurtz, D. M., Jr., and Scott, R. A. (1997) Dissecting contributions to the thermostability of *Pyrococcus furiosus* rubredoxin: $\beta$-Sheet chimeras. *Biochemistry 36*, 10406–10413.
7. Bonomi, F., Eidsness, M. K., Iametti, S., Kurtz, D. M., Mazzini, S., and Morleo, A. (2004) Contribution of the $[Fe^{II}(SCys)_4]$ site to the thermostability of rubredoxins. *J. Biol. Inorg. Chem. 9*, 297–306.
8. Bonomi, F., Fessas, D., Iametti, S., Kurtz, D. M., Jr., and Mazzini, S. (2000) Thermal stability of *Clostridium pasteurianum* rubredoxin: Deconvoluting the contributions of the metal site and the protein. *Protein Sci. 9*, 2413–2426.
9. Bonomi, F., Burden, A. E., Eidsness, M. K., Fessas, D., Iametti, S., Kurtz, D. M., Jr., Mazzini, S., Scott, R. A., and Zeng, Q. (2002) Thermal stability of the $[Fe(SCys)_4]$ site in *Clostridium pasteurianum* rubredoxin: Contributions of the local environment and Cys ligand protonation. *J. Biol. Inorg. Chem. 7*, 427–436.
10. Lazaridis, T., Lee, I., and Karplus, M. (1997) Dynamics and unfolding pathways of a hyperthermophilic and a mesophilic rubredoxin. *Protein Sci. 6*, 2589–2605.
11. Strop, P., and Mayo, S. L. (2000) Contribution of surface salt bridges to protein stability. *Biochemistry 39*, 1251–1255.
12. Bonomi, F., Iametti, S., Ferranti, P., Kurtz, D. M., Jr., Morleo, A., and Ragg, E. M. (2008) "Iron priming" guides folding of denatured aporubredoxins. *J. Biol. Inorg. Chem. 13*, 981–991.
13. Roder, H., Maki, K., and Cheng, H. (2006) Early events in protein folding explored by rapid mixing methods. *Chem. Rev. 106*, 1836–1861.
14. Wilson, C. J., Apiyo, D., and Wittung-Stafshede, P. (2004) Role of cofactors in metalloprotein folding. *Q. Rev. Biophys. 37*, 285–314.
15. Eidsness, M. K., Burden, A. E., Richie, K. A., Kurtz, D. M., Jr., Scott, R. A., Smith, E. T., Ichiye, T., Beard, B., Min, T., and Kang, C. (1999) Modulation of the redox potential of the $[Fe(SCys)_4]$ site in rubredoxin by the orientation of a peptide dipole. *Biochemistry 38*, 14803–14809.
16. Zeng, Q., Smith, E. T., Kurtz, D. M., Jr., and Scott, R. A. (1996) Protein determinants of metal site reduction potentials: Site-directed mutagenesis studies of *Clostridium pasteurianum* rubredoxin. *Inorg. Chim. Acta 242*, 245–251.
17. Eidsness, M. K., O'Dell, S. E., Kurtz, D. M., Jr., Robson, R. L., and Scott, R. A. (1992) Expression of a synthetic gene coding for the amino acid sequence of *Clostridium pasteurianum* rubredoxin. *Protein Eng. 5*, 367–371.

18. Christensen, H. E., Hammerstad-Pedersen, J. M., Holm, A., Iversen, G., Jensen, M. H., and Ulstrup, J. (1994) Synthesis and characterization of *Desulfovibrio gigas* rubredoxin and rubredoxin fragments. *Eur. J. Biochem. 224*, 97–101.
19. Lombardi, A., Marasco, D., Maglio, O., Di Costanzo, L., Nastri, F., and Pavone, V. (2004) Miniaturized metalloproeins: Application to iron-sulfur proteins. *Proc. Natl. Acad. Sci. U.S.A. 97*, 11923–11927.
20. Ueyama, N., Nakata, M., Fuji, M. A., Terakawa, T., and Nakamura, A. (1985) Analogs of reduced rubredoxin: Positive shifts of redox potentials of cysteine-containing peptide iron(II) complexes. *Inorg. Chem. 24*, 2190–2196.
21. Petros, A. K., Reddi, A. R., Kennedy, M. L., Hyslop, A. G., and Gibney, B. R. (2006) Femtomolar Zn(II) affinity in a peptide-based ligand designed to model thiolate-rich metalloprotein active sites. *Inorg. Chem. 45*, 9941–9958.
22. Xiao, Z., Lavery, M. J., Ayhan, M., Scrofani, S. D. B., Wilce, M. C. J., Guss, J. M., Tregloan, P. A., George, G. N., and Wedd, A. G. (1998) The rubredoxin from *Clostridium pasteurianum*: Mutation of the iron cysteinyl ligands to serine. Crystal and molecular structures of oxidized and dithionite-treated forms of the Cys42Ser mutant. *J. Am. Chem. Soc. 120*, 4135–4150.
23. Xiao, Z. G., Gardner, A. R., Cross, M., Maes, E. M., Czernuszewicz, R. S., Sola, M., and Wedd, A. G. (2001) Redox thermodynamics of mutant forms of the rubredoxin from *Clostridium pasteurianum*: Identification of a stable $Fe^{III}(S\text{-}Cys)_3(OH)$ centre in the C6S mutant. *J. Biol. Inorg. Chem. 6*, 638–649.
24. Zartler, E. R., Jenney, F. E., Terrell, M., Eidsness, M. K., Adams, M. W. W., and Prestegard, J. H. (2001) Structural basis for thermostability in aporubredoxins from *Pyrococcus furiosus* and *Clostridium pasteurianum*. *Biochemistry 40*, 7279–7290.
25. Busenlehner, L. S., Apuy, J. L., and Giedroc, D. P. (2002) Characterization of a metalloregulatory bismuth(III) site in *Staphylococcus aureus* pI258 CadC repressor. *J. Biol. Inorg. Chem. 7*, 551–559.
26. Blindauer, C. A., and Sadler, P. J. (2005) How to hide zinc in a small protein. *Acc. Chem. Res. 38*, 62–69.
27. Ditargiani, R. C., Lee, S. J., Wassink, S., and Michel, S. L. J. (2006) Functional characterization of iron-substituted tristetraprolin-2D (TTP-2D, NUP475-2D): RNA binding affinity and selectivity. *Biochemistry 45*, 13641–13649.
28. Silaghi-Dumitrescu, R., Coulter, E. D., Das, A., Ljungdahl, L. G., Jameson, G. N. L., Huynh, B. H., and Kurtz, D. M. (2003) A flavodiiron protein and high molecular weight rubredoxin from *Moorella thermoacetica* with nitric oxide reductase activity. *Biochemistry 42*, 2806–2815.
29. Iyer, R. B., Silaghi-Dumitrescu, R., Kurtz, D. M., and Lanzilotta, W. N. (2005) High-resolution crystal structures of *Desulfovibrio vulgaris* (Hildenborough) nigerythrin: Facile, redox-dependent iron movement, domain interface variability, and peroxidase activity in the rubrerythrins. *J. Biol. Inorg. Chem. 10*, 407–416.
30. Bitto, E., Bingman, C. A., Bittova, L., Kondrashov, D. A., Bannen, R. M., Fox, B. G., Markley, J. L., and Phillips, G. N. (2008) Structure of human J-type co-chaperone HscB reveals a tetracysteine metal-binding domain. *J. Biol. Chem. 283*, 30184–30192.
31. Proudfoot, M., Sanders, S. A., Singer, A., Zhang, R., Brown, G., Binkowski, A., Xu, L., Lukin, J. A., Murzin, A. G., Joachimiak, A., Arrowsmith, C. H., Edwards, A. M., Savchenko, A. V., and Yakunin, A. F. (2008) Biochemical and structural characterization of a novel family of cystathionine $\beta$-synthase domain proteins fused to a Zn ribbon-like domain. *J. Mol. Biol. 375*, 301–315.
32. Taylor, P. K., Parks, B. A., Kurtz, D. M., Jr., and Amster, I. J. (2001) Analysis of metal incorporation during overexpression of *Clostridium pasteurianum* rubredoxin by electrospray FTICR mass spectrometry. *J. Biol. Inorg. Chem. 6*, 201–206.
33. Bonomi, F., Iametti, S., Kurtz, D. M., Ragg, E. M., and Richie, K. A. (1998) Direct metal ion substitution at the $[M(SCys)_4]^{2-}$ site of rubredoxin. *J. Biol. Inorg. Chem. 3*, 595–605.
34. Ellis, R. J. (2001) Macromolecular crowding: An important but neglected aspect of the intracellular environment. *Curr. Opin. Struct. Biol. 11*, 114–119.
35. Ball, P. (2008) Water as an active constituent in cell biology. *Chem. Rev. 108*, 74–108.
36. Stagg, L., Zhang, S. Q., Cheung, M. S., and Wittung-Stafshede, P. (2007) Molecular crowding enhances native structure and stability of $\alpha/\beta$ protein flavodoxin. *Proc. Natl. Acad. Sci. U.S.A. 104*, 18976–18981.
37. Cabrita, L. D., Dobson, C. M., and Christodoulou, J. (2010) Protein folding on the ribosome. *Curr. Opin. Struct. Biol. 20*, 33–45.